In-silico clinical trial using high performance computational modeling of a virtual human cardiac population to assess drug-induced arrhythmic risk

Jazmin Aguado-Sierra[1], Constantine Butakoff[2], Renee Brigham[4], Apollo Baron[2], Guillaume Houzeaux[1,2], Jose M. Guerra [3], Francesc Carreras[3], David Filgueiras-Rama[5], Paul A. Iaizzo[4], Tinen L. Iles[4], Mariano Vazquez[1,2]

1. Barcelona Supercomputing Center, Barcelona, Spain
2. Elem Biotech S.L., Barcelona, Spain
3. Hospital de la Santa Creu i Sant Pau, Universitat Autónoma de Barcelona, CIBERCV, Barcelona, Spain
4. Visible Heart® Laboratories, Department of Surgery and the Institute for Engineering in Medicine, University of Minnesota, Minneapolis, United States
5. Fundación Centro Nacional de Investigaciones Cardiovasculares (CNIC), Instituto de Investigación Sanitaria del Hospital Clínico San Carlos (IdISSC), CIBERCV, Madrid, Spain

Abstract

Drug-induced arrhythmia continues to be a major health issue worldwide. The need for reliable pro-arrhythmic predictors became relevant during early phases of the SarsCoV2 pandemic, when it was uncertain whether the use of hydroxychloroquine (HCQ) and azithromycin (AZM) could be more harmful than beneficial due to their reported pro-arrhythmic effects.

In this work we describe a computational framework that employs a gender-specific, in-silico cardiac population to assess cardiac drug-induced QT-prolongation after the administration of a single or a combination of potentially cardiotoxic drugs as HCQ and AZM. This novel computational methodology is capable of reproducing the complex behavior of the clinical electrocardiographic response to drug-induced arrhythmic risk, in-silico. Using high performance computing, the computational framework allows the estimation of the arrhythmic risk in a population, given a variety of doses of one or more drugs in a timely manner and providing markers that can be directly related to the clinical scenario. The pro-arrhythmic behavior observed in subjects within the in-silico trial, was also compared to supplemental in-vitro experiments on a reanimated swine hearts. Evidence of transmurally heterogeneous action potential prolongation after the administration of a large dose of HCQ was an observed mechanism of arrhythmia, both in the in-vitro and the in-silico model. The virtual clinical trial also provided remarkably similar results to recent published clinical data. In conclusion, the in-silico clinical trial on the cardiac population is capable of reproducing and providing evidence of the normal phenotype variants that produce distinct arrhythmogenic outcomes after the administration of one or various drugs.

Introduction

Drug-induced arrhythmias are a major health issue worldwide [1]. This issue was stressed during the COVID-19 pandemic with the use of potentially pro-arrhythmic drugs and the combination of them as an urgent attempt to provide initial treatments to control the disease [2]. In this context and other clinical situations requiring high-throughput testing, the creation of novel methodologies capable of providing urgent information concerning the cardiotoxic risks of using potentially pro-arrhythmic drugs will provide scientists and physicians a powerful tool in the clinic.

Currently, there are no predictors that can provide critical a-priori information regarding the potential risks for certain patients with normal QTc intervals to develop QT-prolongation after the administration of one or various drugs that may have cardio-toxic side-effects. This need for reliably pro-arrhythmic risk prediction, became relevant during early phases of the SarsCoV2 pandemic, when it was uncertain whether the uses of hydroxychloroquine (HCQ) and/or azithromycin (AZM) could be more harmful, due to their reported cardiotoxic effects. [3, 4].

It is also well documented that males and females present with different risks for drug-induced arrhythmias and QT-interval prolongation due to sex-specific hormones [5,6]. Furthermore, the function of various cardiac ion channels can be significantly modified by environmental conditions (i.e. hormones, electrolyte concentrations and pH), which can in turn have substantial effects on the overall electrical profile. In the case of COVID-19, hypokalemia has been identified as a prevalent condition in patients, which may increase further the risk of QT prolongation [7]. Further, the combined administrations of several drugs increases the complexities for understanding the associated clinical implications; which is consistent with very limited information relative to drug interactions as drug combinations increase. In many cases, these interactions can be characterized according to most logical biophysical assumptions: potentiation or addition.

A variety of computational methods have been an important component for the study and assessment of drug-induced arrhythmias [8, 9, 10, 11]. The work by Yang et al [8] has employed computational methods from the atomistic level to the tissue level. The work by Bottino et al [9] and Beattie et al. [11], include computational simulations up to the the tissue level. The work by Delaunois et al [10] include both experimental assays and 0-D electrophysiology simulations to assess proarrhythmic risk. Other works also include full heart simulations for pro-arrhythmia assessment [21] of a single subject. The present work uses full human heart biventricular anatomies to simulate a human population, addressing the possible differences in human physiology that can determine the proarrhythmic drug-induced response of some individuals. This cardiac population approach represents a major leap towards demonstrating the utility of in-silico clinical trials to provide comparable information to data obtained from clinical trials.

The primordial objective of this work was to create a “normal virtual population”. No established computational methodology existed to achieve that aim. The second objective was to assess if the administration of a single drug or combinations of drugs within this normal population can reproduce the arrhythmic risk observed clinically. A third objective was to employ existent pharmacodynamic and pharmacokinetic information of the two drugs in question and assess if their measured effects when applied to the human virtual population and provided meaningful clinical information regarding cardiotoxicity. The fourth objective was to develop a reliable methodology to identify the risks of cardiotoxicity and classify the responses within the virtual population to the administered drugs. The final objective of this project was to utilize reanimated swine hearts to observe acute arrhythmic features induced by the administrations of high doses of HCQ: i.e., to obtain validation data of our observed arrhythmias in the virtual population. The in-vitro experimentations were also used to observe the functional effects of HCQ administrations and assess the functional recoveries after washout.

In order to achieve the aforementioned objectives, a variety of requirements and hypotheses were defined. The main requirement towards the creation of a virtual population was to include gender-specific ion channel phenotypes [12]; in order to reproduce the gender-specific risks to drug QTc prolongation. The primary needs towards the generation of a human virtual population was to create a diverse ion channel phenotypic description. We hypothesize that the diversity of clinically observed ion channel expressions can resemble the variabilities of ion channel expressions observed

experimentally [13]. We further hypothesize that these same variabilities apply to both male and female genders.

In the present study, the methodology for the administration of drugs followed published data [11]; further it was hypothesized that the combination of the two drugs would have additive effects. The drug doses administered corresponded to the peak plasma concentration of a given oral dose as previously published [14, 16]. The IC50 values (half-maximal inhibitory concentrations) employed were the ones found in the literature, measured in a variety of cell types [15, 16], hypothesizing that their effects would be similar in the human heart.

In order to determine the arrhythmic risk of each subject, a final hypothesis was established, based on clinical case reports of exercise-induced arrhythmias related to the administration of antimalarial drugs [17]. A virtual stress test was performed on this virtual population to further identify their arrhythmic risks.

These main hypotheses represent a gigantic leap from existing experimental single cardiomyocyte data to full cardiac physiologic responses.

Methods

Computational modelling methodology

The detailed biventricular anatomy, of a female human heart, was segmented from high-resolution magnetic resonance imaging (MRI) data; of this ex-vivo perfusion-fixed specimen. This heart was obtained from an organ donor whose heart was deemed not viable for transplant; via the procurement organization, LifeSource (Minneapolis, MN, USA). This specimen remains as part of the Visible Heart® Laboratories' Human Heart Library at the University of Minnesota. The uses of these heart specimens for research and the laboratory was appropriately consented from the donor families, and the research protocol was reviewed by both the University of Minnesota's Institutional Review Board and LifeSource's Research Committee. The heart was cannulated and perfusion-fixed under a pressure of approximately 40 - 50 mmHg, with 10% phosphate buffered formalin; this preserved the specimen in an end-diastolic state. High resolution images of this unique specimen were then acquired via a 3T Siemens scanner: with 0.44 times 0.44 mm in-plane resolution and slice thickness of 1 to 1.7 mm, which provides all detailed endocardial trabeculae and false tendons with $\simeq$1 mm^2 cross sectional area.

Next, a volumetric finite element mesh (of 65.5 million tetrahedral elements) was created, as previously reported [18], with a regular maximum element side length of 400 microns, needed for electrophysiology simulations, using Quartet [19]. The finite element model of electrophysiology employing the monodomain approximation was solved using Alya [20, 21], an in-house, high performance computing code developed at the Barcelona Supercomputing Center. In order to approximate the fast endocardial activations due to the Purkinje network, a fast endocardial layer with a thickness of approximately 400 microns was employed. The existence of this high conduction layer (10x myocardial diffusion) was important to obtain physiological conduction velocities in the epicardium and to achieve a normal range of total activation times. Fiber orientations were defined using a rule-based model recently published by Doste et al [22]. These fiber orientations defined anisotropic activations of the myocardial tissue. The diffusion coefficient defining the anisotropy was obtained after thorough analysis of the total activation times and the epicardial conduction velocities to obtain normal clinical values (D = 0.0037 ms on the fiber direction and 0.0012 ms in the transverse directions). Pseudo-electrocardiograms (pseudo-ECGs) were calculated by locating each

biventricular model within a torso and recording the cardiac electrical activities at three field coordinates (or "electrodes"); positioned at the approximate locations of the right arm (RA), left arm (LA) and left leg (LL). The pseudo-ECGs were calculated as integrals over the spatial gradients of the transmembrane voltages within the biventricular cardiac tissue. Transmural myocyte heterogeneity was considered by assigning different cellular properties to the following parts of the cardiac walls: endocardial (inner 30%), mid-myocardial (middle 40%) and epicardial (outer 30%). The transmural myocyte heterogeneity was applied following the modifications to the endocardial cell type published by O'Hara and Rudy [23]. The locations of the activation regions within the biventricular cavities was set following the work of Durrer [24]. The initial activation regions (IARs) were: ***1-2***. two activation areas on the RV wall, near the insertion of the anterior papillary muscle (A-PM) ***3.*** high anterior para-septal LV area below the mitral valve ***4.*** central area on the left surface of the septum ***5.*** posterior LV para-septal area at ⅓ of the apex-base distance; as shown in Figure 1.

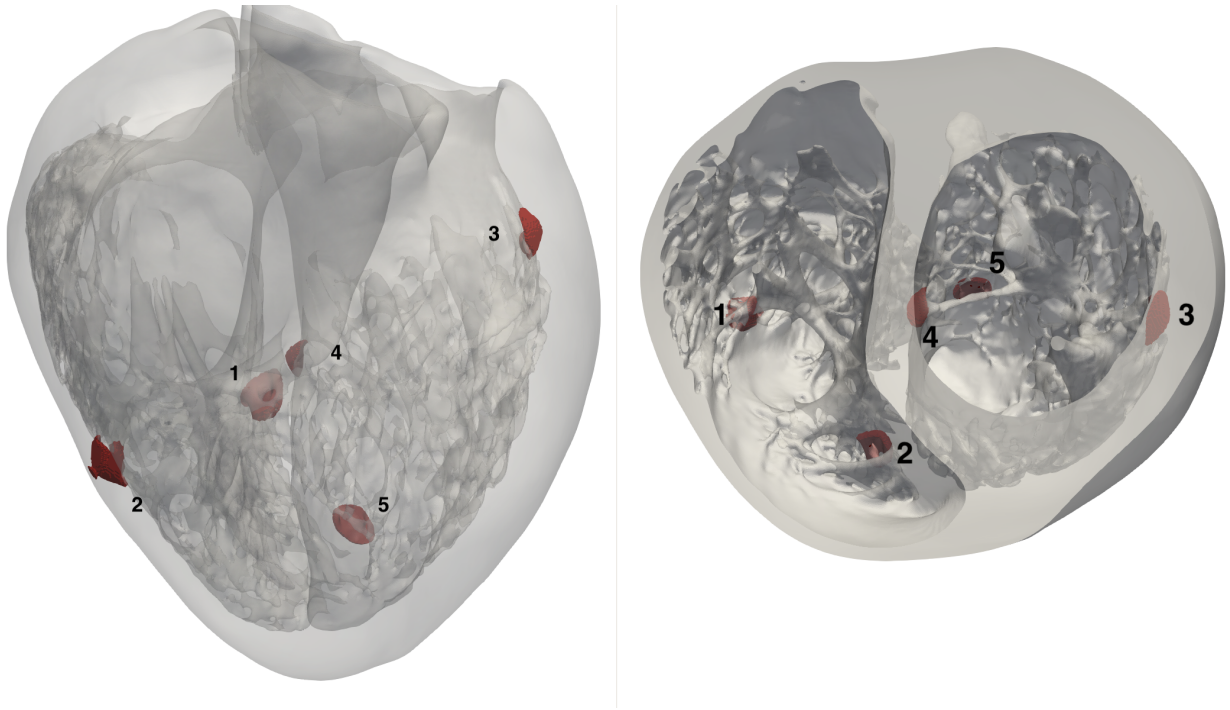

Figure 1. High resolution human biventricular heart anatomy employed. The initial stimuli locations are shown in red.

The O'Hara-Rudy [23] human cardiac ionic model with the conductance modifications to the sodium channel suggested by Dutta [25], and employed by the FDA as the basis for the CiPA initiative for proarrhythmic risk assessment with in-silico and in-vitro methods; this was employed to compute the cardiomyocyte action potentials. Furthermore, in order to study the gender-specific cardiotoxicities within a human heart population, all the changes to ion channels sub-unit expressions listed by Yang PC et al. elsewhere [12], were applied to the cell models to generate both male and female phenotypic cohorts. The spectrum of phenotypes within the developed normal population was set up employing the experimentally-calibrated normal population data published by Muszkiewicz A et al. [13]. Briefly, five ion channels that have the greatest influences on action potential durations were selected: INa, IKr, IKs, ICaL and INaL. The first and third interquartile ranges (values shown in the table A2 in the annex) were varied in a combinatorial manner in order to capture the bounding values of ion channel function. Therefore, the problem was reduced to 2^5 combinations, for a total of 64 subjects, 32 male and 32 female unique cardiomyocyte phenotypes.

The effects of the drugs affecting the ion channel conductances were incorporated following the methodology of Mirams G et al. [26]; using a multi-channel conductance-block formulation for each drug assessed. The plasma concentrations of HCQ were obtained from a pharmacokinetic model published by Collins [14]. Peak concentrations at clinical dosages were employed in these simulations (800 and 400 mg single oral dose of HCQ and combined doses of 200 and 400 mg HCQ and 500 mg AZM). The IC50s on cardiac channels were obtained from published data by Capel [15]. Plasma concentrations and IC50s values for AZM were obtained from published data [16]. All drug-related concentrations and IC50 values employed in this study can be found in table A3 and A4 in the annex. The assumptions regarding the interactions of both drugs were based on the additive effects of each drug on the affected ion channels. This scenario was chosen given that the detailed information about their interactions is currently unknown. Hypokalemia was modelled by reducing the extracellular potassium concentration to 3.2 mmol/L.

The ion channel conductance variations and the drug blocking effects on the ion channel models were solved in a single cell type (endocardial, midmyocardial and epicardial) until steady state of the calcium transient was achieved (given by a measured threshold error of 1e-7 RMS difference between the last 3 beats). From the aforementioned, we obtain the initial conditions to parameterize the finite element mesh. Simulations of 3 to 5 beats were solved at two different basic cycle lengths (BCL): 600 and 400 ms. A total of 896 simulations were run, each one using 640 cores on the Joliot-Curie Rome supercomputer, hosted by GENCI at CEA, France; with computation time provided by the PRACE-COVID-19 fast track pandemic response (project COVID1933). An approximate total of 2.3 million core/hours were employed for this study.

The QTc and QRS values were measured using the three pseudo-ECG leads. Both Framingham and Bazett formulae were used to calculate the QTc from the cohort with a BCL of 600 ms. A surrogate marker for contractility was obtained by calculating the integral of the calcium transient throughout the anatomy. The magnitude of the peak Calcium, the time to peak Calcium, Calcium 90 and the magnitude of the T-wave were also quantified in each simulation. Data were analysed using a custom-made database developed in RStudio [27], and Orange [28]. The relative importances of each phenotype on each marker was assessed using multiple linear regression using RStudio.

The stress test on the population was performed at the BCL of 400 ms (150 bpm). These simulations were employed to assess the arrhythmic risk of each subject. A subject at risk was defined by observing arrhythmic or dangerous rhythms, which included left bundle branch block, ventricular tachycardia or QT-interval greater than 390 ms, which lead to asynchronous activation. The subjects at risk were employed to trace the ion channel kinetics in which arrhythmic events appear.

In Vitro Methodology

In order to assess the acute behaviour of the computational models, an experimental *in-vitro* setup employing reanimated swine hearts was used to assess the electrophysiological and functional effects in response to HCQ administrations.

Recorded Electrical Potentials from Reanimated Hearts

A series of supplemental experiments were performed on a reanimated swine heart utilizing Visible Heart® methodologies. Swine hearts were continuously perfused with a clear, modified Krebs-Henseleit buffer according to previously described methodologies [29, 30]. After providing a single 30 J shock, each heart elicited and sustained an intrinsic rhythm and associated hemodynamic function. This research was ethically approved by the University of Minnesota Institutional Animal Care and Use Committee.

Hydroxychloroquine administration in vitro

Data sets were collected at four separate time points: baseline, during drug infusion of 25 mg of HCQ, after a 10 minute washout period (in which buffer was replaced twice), during a second drug infusion of 25 mg of HCQ and then a final 50 mg infusion of HCQ after another 10 minutes washout period. The drug was prepared by dissolving 25 mg of HCQ in 10L of recirculated buffer and allowed to equilibrate for 2 minutes before data collection. This concentration is equivalent to 7.44 μmol/lt. Dosages were experimentally derived so as to observe the greatest function differential from controls to treatment with HCQ. This protocol was repeated for subsequent doses of HCQ.

Mechanical and Electrical Data Acquisition

Pressure volume loops were measured using clinically available conductance catheters and a data acquisition system (CD Leycom, Netherlands). A conductance catheter was placed in both the left and right ventricle and calibrated to the cardiac function, the data was sampled at a rate of 250Hz at each time point at 10 second intervals. In order to observe local depolarization and relative ion modulations, Monophasic Action Potentials (MAPS) were recorded from both ventricles with MAP4 catheters (Medtronic, Minneapolis, MN, USA) positioned in the RV and LV endocardium and LV anterior epicardium, and the rise time and time to decay were measured for 10 consecutive MAP waveforms for each treatment group. Additionally, 2 decapolar catheters were sutured onto the epicardial surfaces of both ventricles to record the relative changes in electrical activations along the ventricles; in order to capture evidence of dispersion of repolarization. 3-lead surface electrocardiograms were recorded throughout the duration of the study to measure global electrical activities as shown in Figure 2.

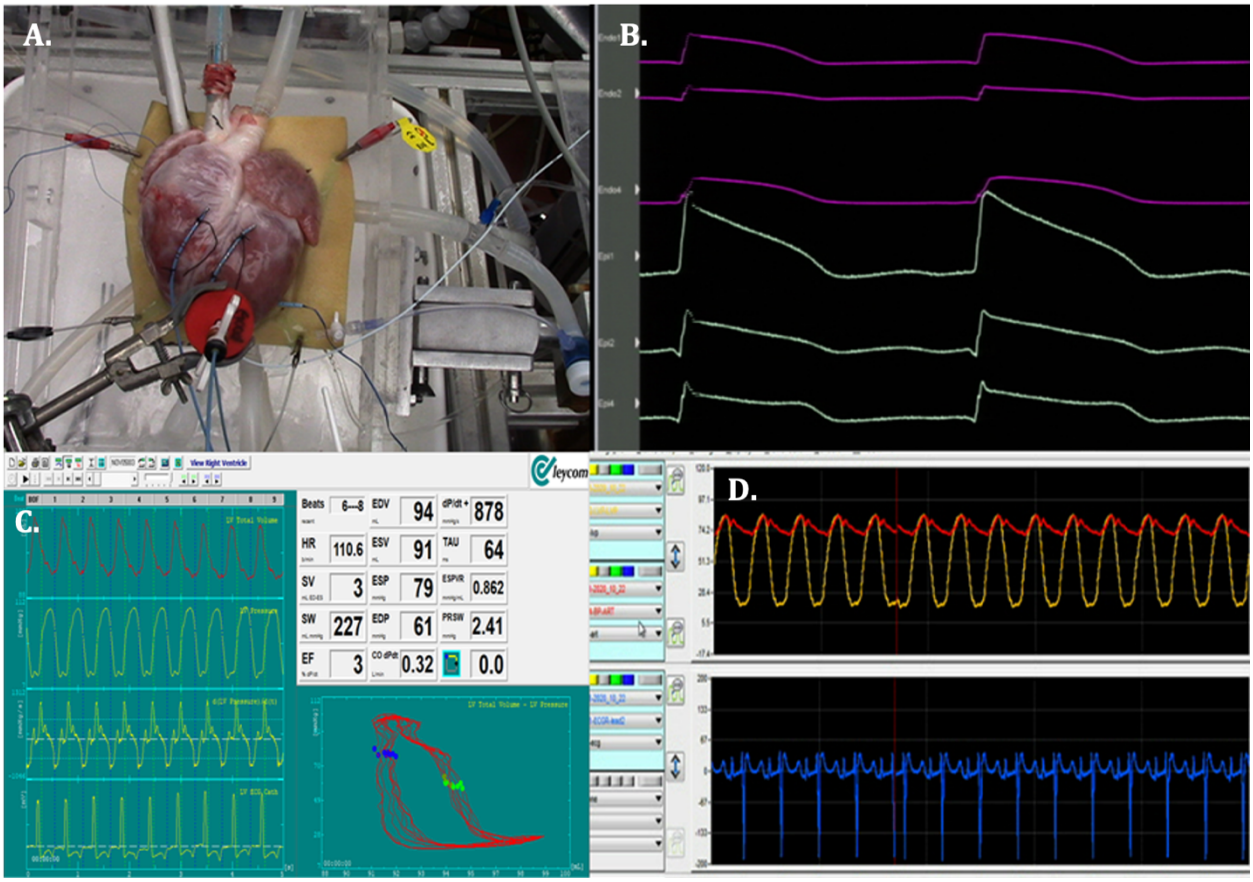

Figure 2: A) An external view of the reanimated swine heart. Two decapolar catheters were sutured to the epicardial surfaces of both the left and right ventricles and a custom device holds the MAPS4 catheter in constant contact with the LV epicardium. B) Electrical activations in LV and RV as measured from decapolar catheters. C) PV loops are measured from conductance catheters placed within both the LV and RV. D) Arterial (red trace) and LV pressures (yellow trace) are recorded along with the 3-lead surface ECG (blue trace)

Results

Computational modelling

All markers measured are shown in Table 1. Both median, interquartile range, mean and standard deviation are reported. The distribution of the data was not normal, however mean and standard deviation is included in order to compare the results to clinically published data.

Marker Median (iqr), mean ± std	Baseline	Hypokalemia (3.2 mmol/L)	HCQ 400 mg	HCQ 800 mg	HCQ 200 mg + AZM 500 mg	HCQ 400 mg + AZM 500 mg	Hypokalemia + HCQ 400 mg + AZM 500 mg
QRS (ms)	102 (98-108) 103.7 ± 4.9	120.4 (114-126) 119.9 ± 6.1	106 (99-109) 104.5 ±5.2	103 (99-109) 104.5 ± 5.2	104.9 (99-109) 104.7 ± 5.3	102 (99-108) 104.5 ± 5.1	119.8 (113-125) 122.9 ± 27.5
QTc Fra	408 (382-	462.3 (435-	456 (430-	476 (455-	429.7 (405-	455 (431-	516.8 (486-

(ms)	434) 409.7 ± 31.9	494) 465.4 ± 37.4	485) 458.8 ± 34.2	504) 479.3 ± 34.9	457) 431.8 ± 32.7	483) 457.8 ± 34.2	547) 523.8 ± 50.8
QTc Baz (ms)	447.5 (413-481) 449.4 ± 41.3	517.2 (482-558) 521.3 ± 48.2	509.3 (476-546) 512.8 ± 44.6	536 (508-571) 539.2 ± 45	475.3 (444-511) 477.9 ± 42.2	508.6 (477-543) 511.5 ± 44.2	587.7 (548-627) 598.4 ± 70
QTc Fra prolongation (ms)	0	54.1 (48-62) 55.7 ± 8.3	48.4 (45-53) 49.1 ± 5.1	70 (64-75) 69.5 ± 7.0	22 (20-23) 22.1 ± 2.4	47.6 (44-51) 48.1 ± 4.7	54.3 (48-60) 58.4 ± 19.2
QTc Baz prolongation (ms)	0	69.9 (62-80) 71.9 ± 10.7	62.4 (58-69) 63.4 ± 6.6	90.3 (82-97) 89.8 ± 9	28.4 (25-30) 28.6 ± 3.1	61.4 (57-66) 62.2 ±6.1	70.1 (63-78) 75.4 ± 24.8
Peak Calcium Integral (mM)	0.283 (0.24-0.35) 0.293 ± 0.087	0.297 (0.234-0.335) 0.291 ± 0.066	0.262 (0.21-0.3) 0.263 ± 0.065	0.250 (0.22-0.28) 0.249 ± 0.056	0.276 (0.212 –0.304) 0.280 ± 0.074	0.260 (0.21-0.3) 0.262 ± 0.065	0.250 (0.203 – 0.295) 0.253 ± 0.049
Time to Peak Calcium Integral (ms)	74 (72-77) 74.7 ± 3.7	82 (78–84) 81.4 ± 3.8	75 (72-77) 74.8 ± 3.9	75 (72-77) 75 ± 3.8	74.5 (72 – 77) 74.9 ± 3.9	75 (72-77) 74.9 ± 4	82 (78 – 84) 82.2 ± 6.1
Calcium 90 (ms)	349 (341-372) 352.7 ± 18.2	373 (359–380) 373.4 ± 19.2	369 (354–381) 369 ± 17	376.5 (361 – 384) 373.9 ± 15.4	358 (346–378) 360.8 ± 17.6	369 (354–381) 369 ± 16.8	386.5 (374–396) 385.5 ± 22.2
T-wave Magnitude (mV)	6.71 (5.6-7.2) 6.45 ± 0.99	8.45 (7.78–8.95) 8.38 ± 0.88	6.28 (5.2-6.6) 6.02 ± 0.86	6.08 (5.1-6.5) 5.82 ± 0.86	6.41 (5.35-6.82) 6.13 ± 0.94	6.24 (5.2-6.6) 5.97 ± 0.87	7.91 (7.11–8.38) 7.81 ± 1.4

Table 1. Median (interquartile range); mean ± standard deviations of all the markers assessed in the entire population at baseline and after the administration of 400 mg and 800 mg of HCQ; and the administration of 400 and 200 mg HCQ combined with 500 mg of AZM.

The QTcFra histogram of the simulated population at baseline and after the administrations of the 800 mg, 400 mg dose of HCQ and the combined use of 400mg of HCQ and 500 mg of AZM are shown in figure 3.

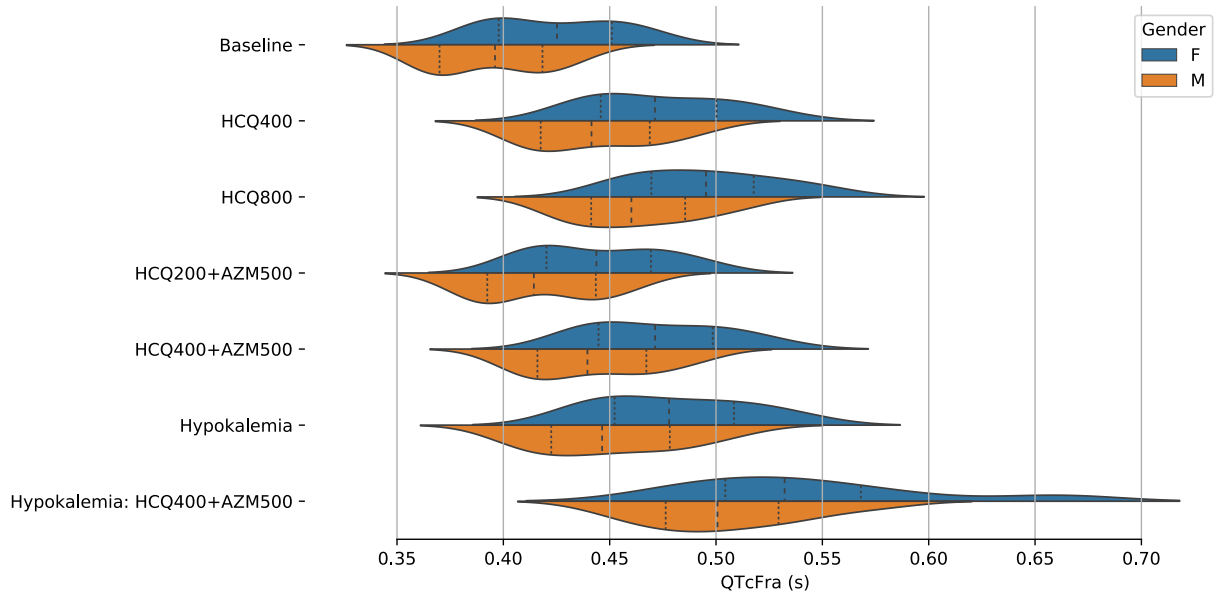

Figure 3. Histogram of the QTc Fra values of the entire population classified by gender during baseline and after the administrations of 400 and 800 mg HCQ and the use of 200 and 400 mg HCQ in combination with 500 mg of AZM under normal conditions and under hypokalemia (3.2 mmol/L)

The QTc prolongation in the entire cohort is shown in figure 4, classified by gender.

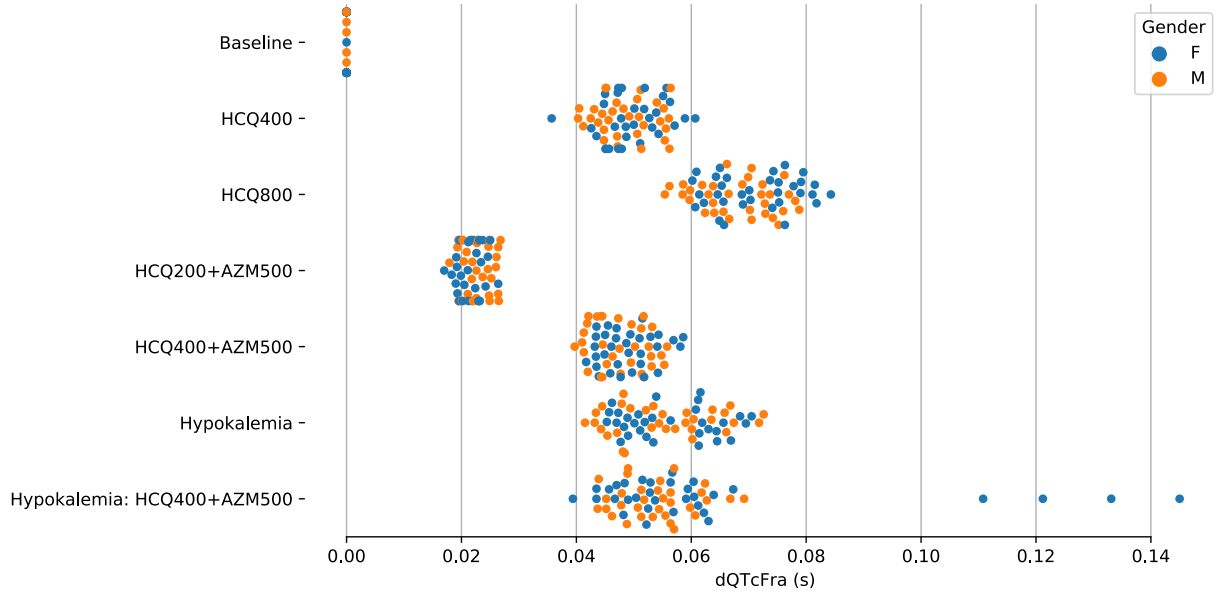

Figure 4. QTc prolongation using Framingham normalization classified by gender.

The solutions for the full cohort after a stress test showed numerous arrhythmic responses that were employed to characterize the risks of drug-induced arrhythmia. For each virtual patient, the resulting QTc Fra after treatment was classified by the risk assessment after the stress test. Results are shown in Figure 5. It is important to note that the virtual clinical study was able to reproduce the complexity

of drug-induced arrhythmia, where QTc was not a definite marker of arrhythmic risk, as it is shown in detail in Figure 6.

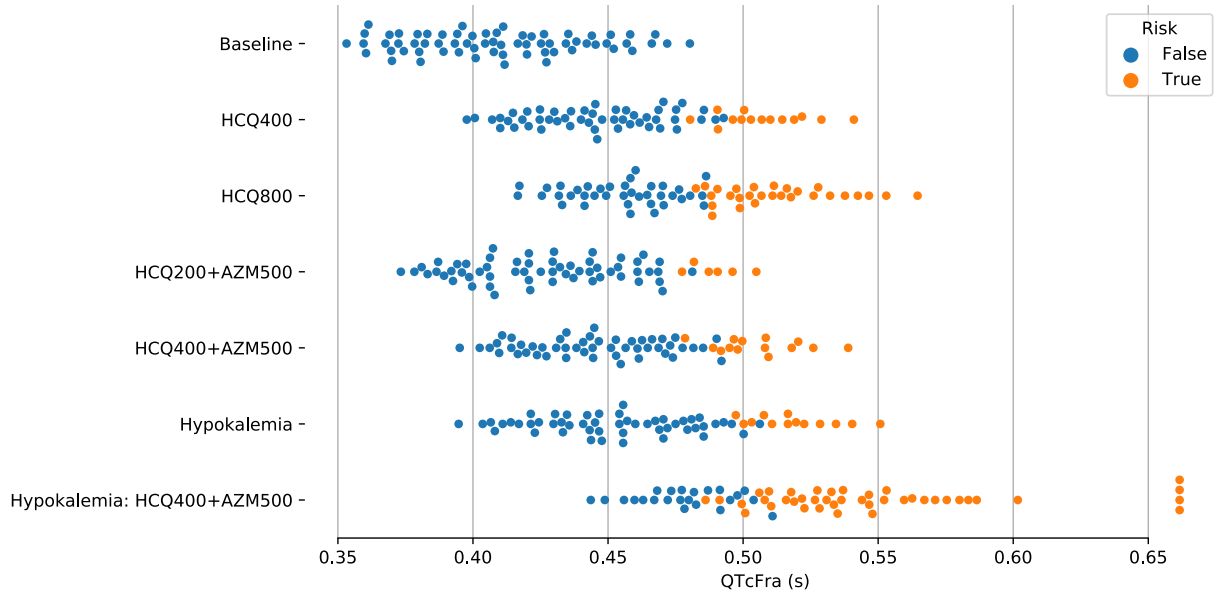

Figure 5. QTc Fra results of all cohorts classified by risk. Subjects at risk of drug-induced arrhythmias are shown in orange.

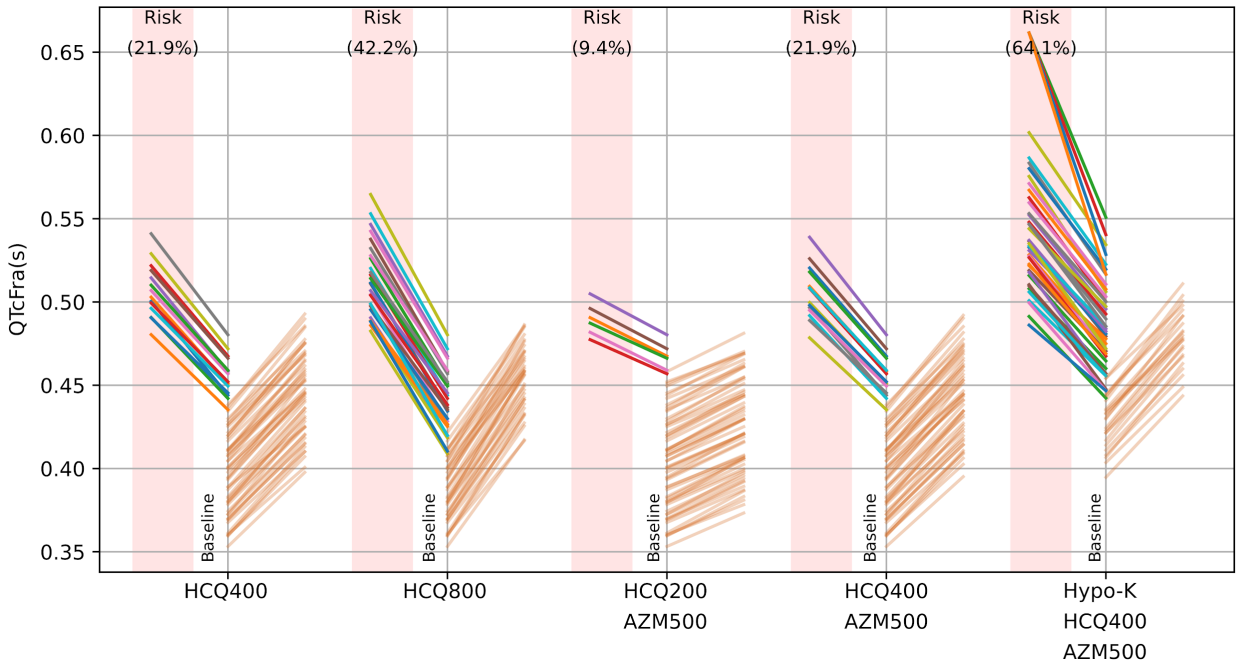

Figure 6. QTcFra prolongation trajectory of each subject of the normal and hypokalemic virtual population after the administration of various doses of HCQ (oral dosis in mg) as sole drug, and in combination with AZM (oral dosis in mg) classified by risk.

The derived virtual subject population had ion channel phenotypic expressions at the first and third quartile ranges of the variabilities of the five main myocardial conductances that affect the action potential durations. Figure 6 shows the progression of each normal and hypokalemic virtual subject after the administrations of the various doses of HCQ and AZM. Notice that the QTc (both Framingham or Bazett) value was not a definite predictor of arrhythmic risk within the simulated cohort, asi it is known to happen in the clinical setting. This precise observation makes the stratification of patients that can develop drug-induced arrhythmias a major unsolved problem. It was observable that two patients with the same QTcFra value could present two distinct responses to drug administration.

The characteristics of the arrhythmic phenotypes were traced back within the baseline population, in order to identify the phenotypes that might exhibit a propensity for a drug-induced arrhythmic behavior. The most common phenotype in the virtual population at high risk, was a low GKr, however not all of the phenotypes with low GKr elicited these arrhythmic scenarios (see figure 7). The relative importance of these currents show that the main current involved in the QTc length was GKr; however, the relative importances for the QTc prolongations after the administrations of the various drug doses, were GKs and GNaL.

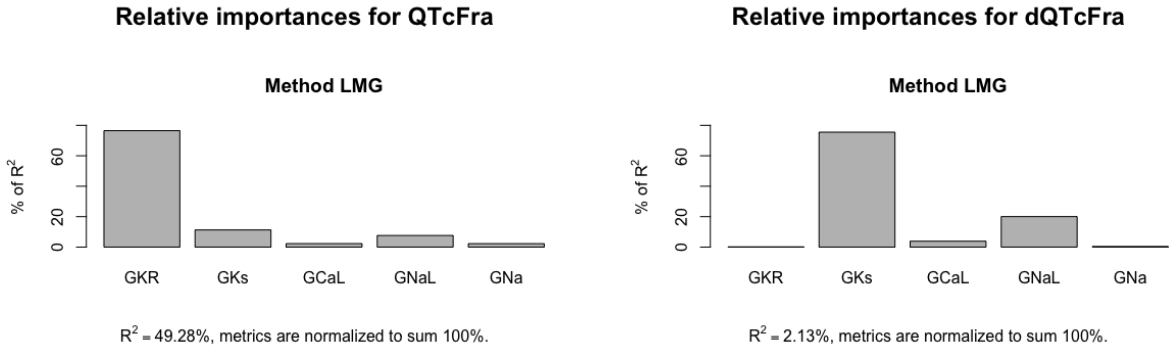

A. B.

Figure 7. Relative importance of the ion channel current conductances on two of the measured markers: A) QTc Fra and B) the prolongation of QTc Fra.

Within this study, QTc was normalized employing both the Framingham and Bazett convention. It is noticeable that both normalizations provide different QTc values. The Bazett convention provides QTc values consistently higher than the Framingham convention at 600 ms bcl; an average 52.5 $\pm$ 15.9 ms higher.

In-vitro experimentation

The recorded in-vitro measurements from the reanimated swine hearts are shown in Table 2.

	BCL (s) mean ± std	LVPsystolic (mmHg) mean ± std	LVPdiastolic (mmHg) mean ± std	dP/dt (mmHg/s) mean ± std	Stroke Work (mL mmHg) mean ± std

Baseline	0.604 ± 0.002	76.9 ± 5.56	18.39 ± 0.39	948.17 ± 289.2	179.48 ± 6.81
25 mg dose 1	0.586 ± 0.135	50.3 ± 9.12	19.99 ± 1.3	396.2 ± 107.63	58.2 ± 27.4
Washout	0.578 ± 0.133	60 ± 10.97	16.43 ± 3.83	597.49 ± 107.14	81.45 ± 30.8
25 mg dose 2	0.598 ± 0.06	87 ± 5.73	30.28 ± 5.07	542.55 ± 125.99	60.8 ± 12
50 mg	0.711± 0.121	49.14 ± 6.5	18.26 ± 7.5	375.66 ± 88.08	61.5 ± 23.2

Table 2. In-vitro functional response to the administration of 7.44 μmol/lt of HCQ and after full drug washout.

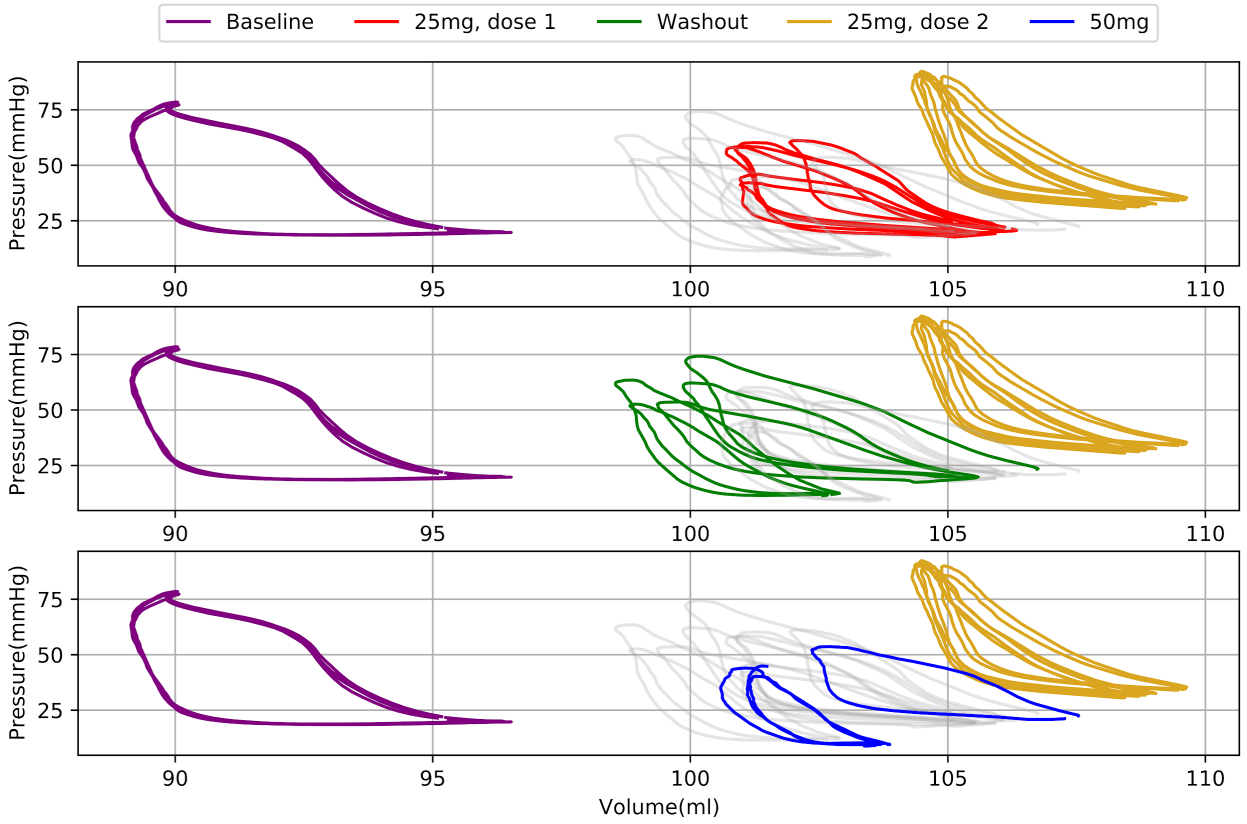

Figure 8. Characteristic left ventricular pressure-volume loops from an ex-vivo perfused,reanimated swine heart at baseline and following administration, washout, and re-administration of HCQ.

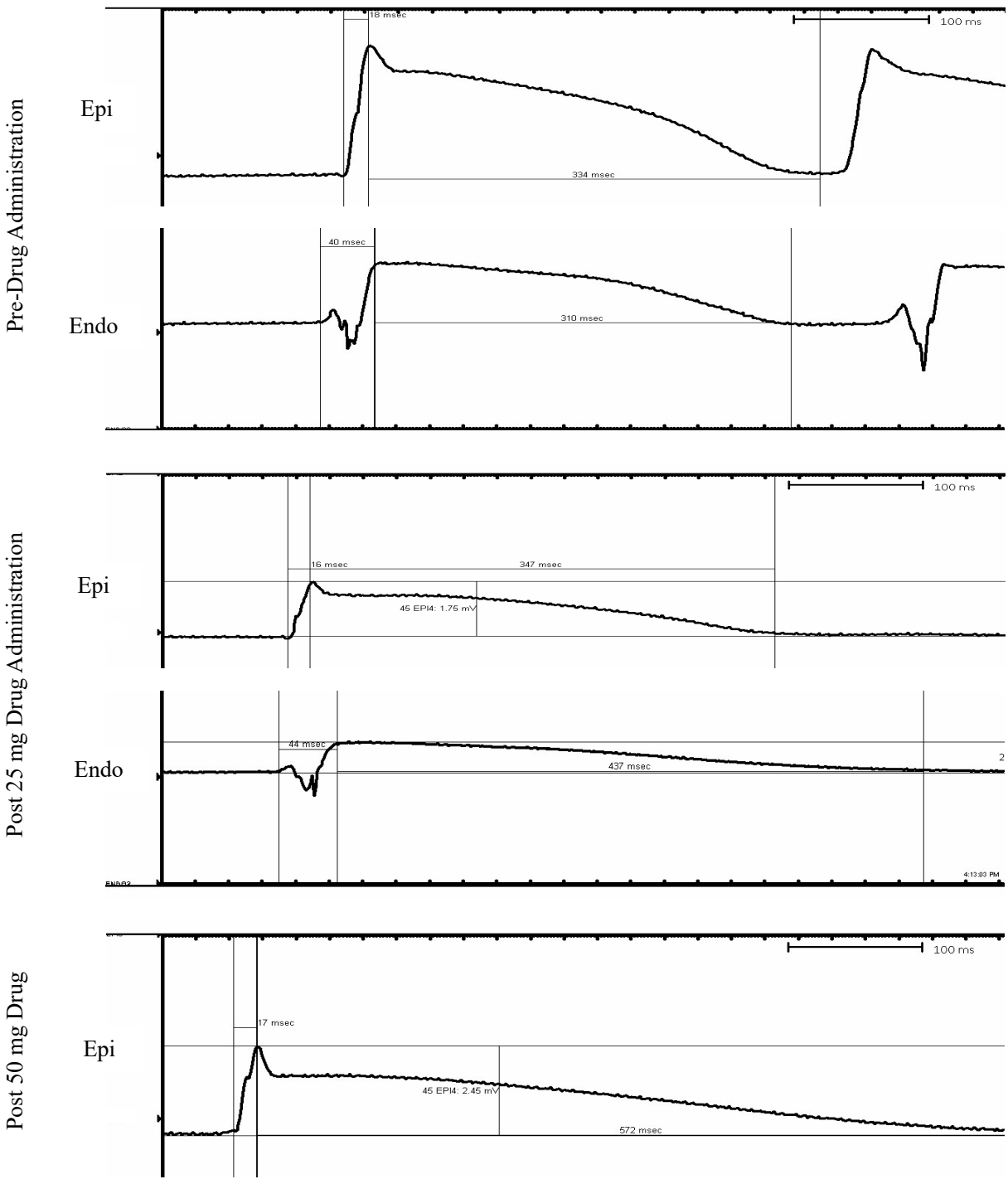

Figure 9. MAPs recorded from the endocardial and epicardial walls of a reanimated swine heart. Note, only epicardial MAPs were able to be recorded for the 50mg HCQ dose.

Monophasic action potentials measured in the ex-vivo swine heart show the approximate APD after the administration of a large dose of HCQ. Epicardial MAP measurements elicited an APD increase after a 25 mg administration of HCQ from 352 to 363 ms (APD prolongation of 11 ms) in the epicardium, and from 350 to 481 ms increase in the endocardium (APD prolongation of 131 ms). For

the extremely high dose of 50 mg (14.88 μmol/lt) the APD in the epicardium increased to 589 ms (APD prolongation of 237 ms). Interestingly, the APD differences between endocardium and epicardium on a virtual subject where LBBB was observed after the administration of 800 mg of HCQ, showed an increase of the AP in the endocardium of an average 0.063 ± 0.0315 s with respect to the epicardium. Measurements are shown in supplemental video S3.

Discussion

To our knowledge, this is one of the first applications of investigating the propensities of administered therapeutic to induce arrhythmias within a "virtual patient population". The developed computational framework employs gender-specific cardiac phenotypes to define this virtual population under both normal and hypokalemic conditions. We specifically sought to identify alterations induced by the administrations of hydroxychloroquine (HCQ) and azithromycin (AZM). We also perform a series of validation experiments on a reanimated swine hearts to assess function and types of arrhythmic risks within an *in vitro* model after HCQ administrations.

The QTc values and QTC prolongations obtained from the computational framework fell within the values observed for normal patients in the clinic. The results were compared to those of clinical studies recently published [31, 32]. In both clinical studies, the Bazett normalization was employed.

The QTc prolongations within the virtual population were approximately within the ranges of the clinical data. Arrhythmic risk as evaluated from the stress test results indicated that 21.8% of the computational cohort exhibited a higher arrhythmic risks after the administrations of a sole dosis of HCQ (400 mg) and the co-administration of HCQ (400 mg) plus AZM (500 mg). For the administration of 200 mg of HCQ plus 500 mg of AZM, the percentage risk fell to 9.3%. The risk increased significantly on subjects with hypokalemia (3.2 mol K+ concentration) to 64% within the virtual population. At a peak plasma concentration after the administration of 800 mg of HCQ, the risk for arrhythmic events was calculated as 43.7%. The virtual clinical trial was able to confirm that the use of HCQ was associated with a proarrhythmic risk, but it did not worsen when it was used in combination with AZM as has been observed clinically and experimentally [10, 31, 32].

QTc Bazett (ms)	Virtual Clinical Trial N= 64 Median [iqr] Mean $\pm$ std	Mercuro et al.[32] N = 90 Median [iqr]	Saleh et al. [31] N = 200 Mean $\pm$ std
Baseline	447.5 [413-481] 449.4 $\pm$ 41.3	455 [430-474]	440.6 $\pm$ 24.9
HCQ 400 mg	509 [476-546] 512.8 $\pm$ 44.6	473 [454-487]	NA
HCQ 200 mg + AZM 500 mg	475 [444-511] 477.9 $\pm$ 42.2	NA	470.4 $\pm$ 45.0
HCQ 400 mg + AZM 500 mg	508 [477-543] 511.5 $\pm$ 44.2	442 [427-461]	NA

Hypokalemia (3.2 mmol) + HCQ 400 mg + AZM 500 mg	587 [548-627] 598.4 $\pm$ 70	NA	NA

Table 3. Comparison of QTc Bazett values between the virtual clinical trial and published clinical trials.

It is important to stress that the concentrations tested within these virtual healthy patients were peak plasma concentrations, therefore representing their effects at a discrete high plasma concentrations, or "worst case" scenarios. These predicted values may change according to the relative metabolisms of these drugs in a clinical setting and according to the interaction with other antiarrhythmic medications. It is important to note that this framework allows for the testing of any plasma concentration of a given drug on cardiac electrophysiology.

Comparison to clinical data published by Saleh et al. [31] is complex, provided that all subjects, even with a variety of potassium concentrations lower than normal, were included within their cohort statistics. However, it is noticeable that ventricular tachycardia occurred on 7 out of 8 of the reported patients with a potassium concentration lower than normal, in agreement to the high risk on the virtual hypokalemic population as shown in Table 4. The match between the percentages of subjects at risk after the administration of 400 mg of HCQ and the combination of 400 mg of HCQ and 500 mg of AZM was remarkable. Interestingly, within the virtual population one could be able to match an approximate behavior of a cohort provided that information of the phenotypic variations are known.

Subjects at Risk (%)	Virtual Clinical Trial N= 64	Mercuro et al. [31] N = 90	Saleh et al. [32] N = 200
HCQ 400 mg	21.8%	19%	NA
HCQ 200 mg + AZM 500 mg	9.3%	NA	3.5%
HCQ 400 mg + AZM 500 mg	21.8%	21%	NA
Hypokalemia (3.2 mmol) + HCQ 400 mg + AZM 500 mg	64%	NA	NA

Table 4. Comparison of the percentage of subjects at risk between the virtual clinical trial and the clinical trials published in the literature.

The *in-vitro* experimentation on the reanimated swine hearts provided evidence for transmural heterogeneous effects of HCQ on action potential durations. This was evidenced by heightened drug-induced transmural heterogeneities, as has been previously associated with multi-channel blocking drugs [32]. Enhanced transmural heterogeneities of focal APs provides an important arrhythmic risk, as observed on one of the subjects that presented an LBBB after the administration of 800 mg of HCQ. This further confirms the capability of the computational models to exhibit the arrhythmic behaviors observed experimentally. Lastly, the long-lasting effects on cardiac function after a complete washout of a large dose of HCQ was an important observation towards the clinical use of HCQ.

Limitations

The IC50 values obtained from the literature [15, 16] to date, have not been quantified on data obtained for human cardiomyocytes; these data come from guinea pig SAN cells and human ion

channels heterologously expressed in human embryonic kidney HEK293 cells. It is however interesting to observe that these values were capable of providing an approximately similar response in our virtual and the recently published clinical trials. The translation of ion channel behaviors between species regarding cardiac ion channel functions remains today, an extremely complex unsolved problem. In this work, we employed the only data available in the literature, as a "naive" approximation. Furthermore, the interactions of two administered cardiotoxic drugs also remains a complex unsolved problem. The 'naive' approach assumed in this work, regarding the additive effect of the two drugs on the ion channel blocking effect, can be revised as emerging research becomes available. Similarly, any of the pharmacokinetics and pharmacodynamics of the drugs employed can be better tuned as data becomes available.

Further, one needs to recognize that the drug effects may differ depending on the relative metabolisms of a given drug, as well as according to the virtual population's phenotypic expressions of cardiac ion channels. The results from these simulations reflect the behaviors of the first and third interquartile ranges in ion channel variabilities, without any comorbidities (i.e. ischemia, other metabolite disturbances, infarction, and/or established cardiac genetic disorders). The assessments of the drug effects on a more broad population remains part of future work. However, the assumptions tested in the present study were able to provide timely critical information concerning phenotypic characteristics of the subset of our virtual subjects that have a higher predisposition to drug-induced QT prolongations.

It is important to point out that this is the first time that a pipeline, like the one presented here, has been created to assess drug cardiotoxicity on human cardiac ventricular electrophysiological behaviors. The use of more detailed ion channel models of herg can be employed in future work.

Conclusions

A virtual gender-specific cohort yielded a range of electrocardiographic phenotypes that resemble a normal human cohort. The computational framework developed was capable of reproducing the effects of one or more administered cardiotoxic drugs, showing remarkable resemblance to published clinical studies. It was capable of reproducing the complexity of the cardiotoxicity response in the human population. Furthermore, it may be employed in future urgent applications to provide primary information about the dosages and the combined effects of drugs; most importantly this has application when clinical guidance is unavailable. The data required for such computational models are the plasma concentrations of the drug or drugs in question and the IC50 values for each of the cardiac ion channels they affect. An in-silico clinical trial framework like the one proposed in this work, could be capable of providing evidence of the proarrhythmic risk of QTc-interval prolonging drugs in a normal or diseased population using high performance computing within a day.

The virtual normal cohort can further be interrogated relative to any population variants that produce a distinct, arrhythmogenic outcome after the administration of one or various drug combinations. This can be exploited towards the identification of more accurate potential markers of cardiotoxicity. The identification of the most prevalent phenotypes within a specific population may further be employed within this computational framework: i.e, to establish predictive bounds of arrhythmogenesis of a relevant, specific sample population.

Acknowledgements

This project has received funding from the European Union's Horizon 2020 research and innovation programme under grant agreements No 823712 (CompBioMed project, phase 2) and No 777204

(SilicoFCM project). Computation time was provided by PRACE-COVID-19 fast track pandemic response (project COVID1933) at the Joliot-Curie Rome supercomputer, hosted by GENCI at CEA, France. JA-S is funded by a Ramon y Cajal fellowship (RYC-2017-22532), MINECO, Spain. CB is funded by the Torres Quevedo Program (PTQ2018-010290), MINECO, Spain.

References:

1. Giselle Sarganas, Edeltraut Garbe, Andreas Klimpel, Rolf C. Hering, Elisabeth Bronder, Wilhelm Haverkamp, Epidemiology of symptomatic drug-induced long QT syndrome and torsade de pointes in Germany, *EP Europace*, Volume 16, Issue 1, January 2014, Pages 101–108, https://doi.org/10.1093/europace/eut214
2. Cavalcanti AB, Zampieri FG, Rosa RG, Azevedo LCP, Veiga VC, Avezum A, Damiani LP, Marcadenti A, Kawano-Dourado L, Lisboa T, Junqueira DLM, de Barros E Silva PGM, Tramujas L, Abreu-Silva EO, Laranjeira LN, Soares AT, Echenique LS, Pereira AJ, Freitas FGR, Gebara OCE, Dantas VCS, Furtado RHM, Milan EP, Golin NA, Cardoso FF, Maia IS, Hoffmann Filho CR, Kormann APM, Amazonas RB, Bocchi de Oliveira MF, Serpa-Neto A, Falavigna M, Lopes RD, Machado FR, Berwanger O; Coalition Covid-19 Brazil I Investigators. Hydroxychloroquine with or without Azithromycin in Mild-to-Moderate Covid-19. N Engl J Med. 2020 Nov 19;383(21):2041-2052. doi: 10.1056/NEJMoa2019014. Epub 2020 Jul 23. Erratum in: N Engl J Med. 2020 Nov 19;383(21):e119. PMID: 32706953; PMCID: PMC7397242.
3. White, Nicholas J. Cardiotoxicity of antimalarial drugs. The Lancet Infectious Diseases, Volume 7, Issue 8, 549-558.
4. Ray, Wayne A. and Murray, Katherine T. and Hall, Kathi and Arbogast, Patrick G. and Stein, C. Michael. Azithromycin and the risk of cardiovascular death. N Engl J Med. 2012. 366(20): 1881--1890.
5. Salama G, Bett GC. Sex differences in the mechanisms underlying long QT syndrome. Am J Physiol Heart Circ Physiol. 2014 Sep 1;307(5):H640-8. doi: 10.1152/ajpheart.00864.2013. Epub 2014 Jun 27. PMID: 24973386; PMCID: PMC4187395.
6. Arja Suzanne Vink, Sally-Ann B. Clur, Arthur A.M. Wilde, Nico A. Blom. Effect of age and gender on the QTc-interval in healthy individuals and patients with long-QT syndrome, Trends in Cardiovascular Medicine, Volume 28, Issue 1, 2018, Pages 64-75.
7. Chen D, Li X, Song Q, Hu C, Su F, Dai J, Ye Y, Huang J, Zhang X. Assessment of Hypokalemia and Clinical Characteristics in Patients With Coronavirus Disease 2019 in Wenzhou, China. JAMA Netw Open. 2020 Jun 1;3(6):e2011122. doi: 10.1001/jamanetworkopen.2020.11122. PMID: 32525548; PMCID: PMC7290402.
8. Yang PC, DeMarco KR, Aghasafari P, Jeng MT, Dawson JRD, Bekker S, Noskov SY, Yarov-Yarovoy V, Vorobyov I, Clancy CE. A Computational Pipeline to Predict Cardiotoxicity: From the Atom to the Rhythm. Circ Res. 2020 Apr 10;126(8):947-964. doi: 10.1161/CIRCRESAHA.119.316404. Epub 2020 Feb 24. PMID: 32091972; PMCID: PMC7155920.
9. Bottino D, Penland RC, stamps A, Traebert M, Dumotier B, Georgiva A, Helmlinger G, Lett GS. Preclinical cardiac safety assessment of pharmaceutical compounds using an integrated systems-based computer model of the heart. Prog Biophys Mol Biol. 2006 Jan-Apr;90(1-3):414-43. doi: 10.1016/j.pbiomolbio.2005.06.006. PMID: 16321428.
10. Delaunois A, et al. Applying the CiPA approach to evaluate cardiac proarrhythmia risk of some antimalarials used of-label in the first wave of COVID-19. Clinical and Translational Science. Accepted Author Manuscript. Https://doi.org/10.1111/cts.13011

11. Beattie KA, Luscombe C, Williams G, Munoz-Muriedas J, Gavaghan DJ, Cui Y, Mirams GR. Evaluation of an in silico cardiac safety assay: using ion channel screening data to predict QT interval changes in the rabbit ventricular wedge. J Pharmacol Toxicol Methods. 2013 Jul-Aug;68(1):88-96. doi: 10.1016/j.vascn.2013.04.004. Epub 2013 Apr 25. PMID: 23624022; PMCID: PMC4142193.
12. Yang PC, Clancy CE. In silico Prediction of Sex-Based Differences in Human Susceptibility to Cardiac Ventricular Tachyarrhythmias. Front Physiol. 2012 Sep 14;3:360. doi: 10.3389/fphys.2012.00360. PMID: 23049511; PMCID: PMC3442371.
13. Muszkiewicz A, Britton OJ, Gemmell P, Passini E, Sánchez C, Zhou X, Carusi A, Quinn TA, Burrage K, Bueno-Orovio A, Rodriguez B. Variability in cardiac electrophysiology: Using experimentally-calibrated populations of models to move beyond the single virtual physiological human paradigm. Prog Biophys Mol Biol. 2016 Jan;120(1-3):115-27. doi: 10.1016/j.pbiomolbio.2015.12.002. Epub 2015 Dec 14. PMID: 26701222; PMCID: PMC4821179.
14. Collins KP, Jackson KM, Gustafson DL. Hydroxychloroquine: A Physiologically-Based Pharmacokinetic Model in the Context of Cancer-Related Autophagy Modulation. J Pharmacol Exp Ther. 2018 Jun;365(3):447-459. doi: 10.1124/jpet.117.245639. Epub 2018 Feb 8. PMID: 29438998; PMCID: PMC5931434.
15. Capel RA, Herring N, Kalla M, Yavari A, Mirams GR, Douglas G, Bub G, Channon K, Paterson DJ, Terrar DA, Burton RA. Hydroxychloroquine reduces heart rate by modulating the hyperpolarization-activated current If: Novel electrophysiological insights and therapeutic potential. Heart Rhythm. 2015 Oct;12(10):2186-94. doi: 10.1016/j.hrthm.2015.05.027. Epub 2015 May 27. PMID: 26025323; PMCID: PMC4689153.
16. Yang Z, Prinsen JK, Bersell KR, Shen W, Yermalitskaya L, Sidorova T, Luis PB, Hall L, Zhang W, Du L, Milne G, Tucker P, George AL Jr, Campbell CM, Pickett RA, Shaffer CM, Chopra N, Yang T, Knollmann BC, Roden DM, Murray KT. Azithromycin Causes a Novel Proarrhythmic Syndrome. Circ Arrhythm Electrophysiol. 2017 Apr;10(4):e003560. doi: 10.1161/CIRCEP.115.003560. PMID: 28408648; PMCID: PMC5396181.
17. Fourcade L, Camus O, Roche N, Chenilleau MC, Gil JM, Massoure PL. Bloc de branche gauche douloureux d'effort associé à la chimioprophylaxie antipaludique par chloroquine [Exercise-induced left bundle branch block with chest pain related to antimalarial prophylaxis with chloroquine]. Med Sante Trop. 2014 Jul-Sep;24(3):320-2. French. doi: 10.1684/mst.2014.0338. PMID: 24919211.
18. Sacco, Federica. Quantification of the influence of detailed endocardial structures on human cardiac haemodynamics and electrophysiology using HPC. 2019. http://hdl.handle.net/10803/667670
19. C. Doran. Isosurface Stuffing Improved; acute lattices and feature matching. Master's Thesis, University of British Columbia, 2013
20. A. Santiago, J. Aguado-Sierra, M. Zavala-Aké, R. Doste-Beltran, . Fully coupled fluid-electro-mechanical model of the human heart for supercomputers. International journal for numerical methods in biomedical engineering 34.12 (2018): e3140.
21. Margara, Francesca, et al. "In-silico human electro-mechanical ventricular modelling and simulation for drug-induced pro-arrhythmia and inotropic risk assessment." Progress in biophysics and molecular biology 159 (2021): 58-74.
22. Doste R, Soto-Iglesias D, Bernardino G, Alcaine A, Sebastian R, Giffard-Roisin S, Sermesant M, Berruezo A, Sanchez-Quintana D, Camara O. A rule-based method to model myocardial fiber orientation in cardiac biventricular geometries with outflow tracts. Int J Numer Method Biomed Eng. 2019 Apr;35(4):e3185. doi: 10.1002/cnm.3185. Epub 2019 Feb 19. PMID: 30721579.

23. T. O'Hara, L. Virag, A. Varro, Y. Rudy, Simulation of the undiseased human cardiac ventricular action potential: Model formulation and experimental validation, PLOS Comput. Biol. 7 (2011) 1–29.
24. D. Durrer, R. Dam, G. E. Freud, M.J. Janse, F.L. Meijler, R.C. Arzbaecher. Total excitation of the isolated human heart, Circulation 6 (1970) 899 – 912.
25. S. Dutta, A. Minchoĺe, T. A. Quinn, B. Rodriguez, Electrophysiological properties of computational human ventricular cell action potential models under acute ischemic conditions, Progress in Biophysics and Molecular Biology 129 (2017) 40 – 52. Validation of Computer Modelling.
26. Mirams GR, Cui Y, Sher A, Fink M, Cooper J, Heath BM, McMahon NC, Gavaghan DJ, Noble D. Simulation of multiple ion channel block provides improved early prediction of compounds' clinical torsadogenic risk. Cardiovasc Res. 2011 Jul 1;91(1):53-61. doi: 10.1093/cvr/cvr044. Epub 2011 Feb 7. PMID: 21300721; PMCID: PMC3112019.
27. RStudio Team (2020). RStudio: Integrated Development for R. RStudio, PBC, Boston, MA URL http://www.rstudio.com/.
28. Demsar J, Curk T, Erjavec A, Gorup C, Hocevar T, Milutinovic M, Mozina M, Polajnar M, Toplak M, Staric A, Stajdohar M, Umek L, Zagar L, Zbontar J, Zitnik M, Zupan B (2013) Orange: Data Mining Toolbox in Python, Journal of Machine Learning Research 14(Aug): 2349−2353.
29. Chinchoy, Edward, Soule, Charles L., Houlton, Andew J., Gallagher, William J., Hjelle, Mark A., Laske, Timothy G., Morissette, Josée, and Iaizzo, Paul A. Isolated Four-Chamber Working Swine Heart Model. Annals of Thoracic Surgery Vol. 70 No .5 (2000): pp. 1607–1614.
30. Schmidt MM, Iaizzo PA. The Visible Heart® project and methodologies: novel use for studying cardiac monophasic action potentials and evaluating their underlying mechanisms. Expert Rev Med Devices. 2018 Jul;15(7):467-477. doi: 10.1080/17434440.2018.1493922. Epub 2018 Jul 10. PMID: 29989510.
31. Saleh M, Gabriels J, Chang D, Soo Kim B, Mansoor A, Mahmood E, Makker P, Ismail H, Goldner B, Willner J, Beldner S, Mitra R, John R, Chinitz J, Skipitaris N, Mountantonakis S, Epstein LM. Effect of Chloroquine, Hydroxychloroquine, and Azithromycin on the Corrected QT Interval in Patients With SARS-CoV-2 Infection. Circ Arrhythm Electrophysiol. 2020 Jun;13(6):e008662. doi: 10.1161/CIRCEP.120.008662. Epub 2020 Apr 29. PMID: 32347743; PMCID: PMC7299095.
32. Mercuro NJ, Yen CF, Shim DJ, Maher TR, McCoy CM, Zimetbaum PJ, Gold HS. Risk of QT Interval Prolongation Associated With Use of Hydroxychloroquine With or Without Concomitant Azithromycin Among Hospitalized Patients Testing Positive for Coronavirus Disease 2019 (COVID-19). JAMA Cardiol. 2020 May 1:e201834. doi: 10.1001/jamacardio.2020.1834. Epub ahead of print. PMID: 32356863; PMCID: PMC7195692.
33. Zhao, P., Li, P. Transmural and rate-dependent profiling of drug-induced arrhythmogenic risks through in silico simulations of multichannel pharmacology. *Sci Rep* 9, 18504 (2019). https://doi.org/10.1038/s41598-019-55032-x

Annex A.

Table A1. Clinical History of the human heart anatomy employed.

Gender	Age Range	BMI	Cardiac Medical History	Systemic Medical History
Female	20-30	31	None known	None known

Table A2. Scaling factors by which each ion channel is modified in a combinatorial manner.

	GKr	GKs	GNaL	GNa	GCaL
Q1	0.8	0.75	0.75	0.8	0.75
Q3	1.25	1.25	1.25	1.2	1.25

Table A3. Plasma concentrations employed for each oral dose tested (obtained from 13 and 15).

Oral Doses	Peak Plasma Concentration (μmol/lt)
HCQ 200 mg	1.19
HCQ 400 mg	2.97
HCQ 800 mg	4.7
AZM 500 (3-day)	0.59

Table A4. IC50 values for each channel affected by HCQ and AZM. Data obtained from [14,15].

Drug	IKr IC50 (μmol)	ICaL IC50 (μmol)	IKs IC50 (μmol)	INa IC50 (μmol)	IK1 IC50 (μmol)	INaL IC50 (μmol)
HCQ	5.57	22	none	none	none	none
AZM (chronic effect)	219	66.5	184	53.3	43.8	62.2